**Title page**

# Investigation into the effect of beam shape on melt pool characteristics using analytical modelling

**N. Ahmed, K.T. Voisey, D.G. McCartney**
Materials, Mechanics and Structures Research Division, Faculty of Engineering, University of Nottingham, NG7 2RD, UK.

**Corresponding author:**

K.T. Voisey

katy.voisey@nottingham.ac.uk

tel: +44 (0)115 951 4139

# Investigation into the effect of beam shape on melt pool characteristics using analytical modelling

**N. Ahmed, K.T. Voisey, D.G. McCartney**
Materials, Mechanics and Structures Research Division, Faculty of Engineering, University of Nottingham, UK.

## Abstract

An established analytical model is used to simulate an extended laser beam. Multiple Gaussian sources are superimposed to form a rectangular beam and results are compared with a single circular Gaussian source model as well as experimental results from a high power diode laser with a rectangular beam. Melt depth, and melt pool profile and progression have been predicted by modelling which are compared with experimental results from melting of Inconel 625. The model produced is shown to give a reasonable prediction of melt pool shape and can be usefully employed to help optimise overlap required for laser surface processing applications. The value of absorptivity used in the model can be used as a fitting parameter to optimise the match between experimental and predicted results.

Keywords: Analytical modelling, laser surface melting, diode laser, Inconel 625, melt depth, melt pool profile

## 1. Introduction

It is generally accepted that laser surface melting (LSM) can be used for improvement of material properties such as corrosion performance [1]. Large area surface coverage requires overlapping of adjacent tracks. As the extent of overlap increases so too does process time and cost. In addition to this, the overlap zone will be subjected to an additional heat treatment which may result in differences in microstructure. As the corrosion performance is very sensitive to inhomogeneities, therefore significant overlap may degrade the corrosion properties [1-3]. To minimise process cost and any degradation in corrosion resistance, the laser parameters should be selected to produce the desired melt depth with minimal overlapping. These parameters can be selected either by experimental trials or, alternatively, by using an appropriate mathematical model.

Many analytical solutions are found in the literature for modelling heat flow in case of a scanning distributed laser beam. A widely used approach is to integrate the point-source solution over the beam area, a method which involves complex computations. However, if rigorous solutions are not deemed necessary, a simpler, approximate, model such as that developed Ashby et al. [4] and Shercliff et al. [5] can be used. Their simplified approach involved combining and modifying solutions by Rykalin et al. [6] and Bass [7]. To date, this model has mostly been used in the transformation hardening of materials [8, 9], nevertheless good agreement between predicted and experimental results has also been seen for surface melting [10].

In this work, a rectangular high power diode laser beam is used to melt the surface of Inconel 625. The above mentioned approximate model (hereinafter called the Shercliff-Ashby-Easterling or the SAE model) is used to simulate the experimental beam geometry and process parameters. The effect of different beam shapes is modelled and compared with experimental results.

## 2. Experimental methods

The experimental work was carried out with an industrial high power diode laser (HPDL) ROFIN-SINAR DL 025 which has a wavelength of 940 nm. The beam had a rectangular spot size (~6×3 mm) and was focused on the surface of wrought Inconel 625, a nickel based alloy. The diode laser had a top hat intensity distribution along the 6 mm edge and a Gaussian distribution along the 3 mm edge. The relative movement between the sample and beam was parallel to the 3 mm edge so that the melt width was determined by the 6 mm (top hat) dimension of the beam. Three power settings, 1 kW, 1.5 kW, 2 kW, were used and the beam speed was varied in the range of 500-2000 mm $min^{-1}$ for each power.

Polished cross sectional samples from the laser treated region were etched by immersion in aqua-regia (3 parts HCl, 1 part $HNO_3$). Microstructural examination was performed using optical (Keyence VHX-100) and scanning electron microscopy (Philips XL30).

## 3. The Shercliff-Ashby-Easterling (SAE) model

The model details can be found in the literature [4, 5]. In summary, Rykalin et al. [6] provided an analytical solution for the temperature field by considering the beam as a Gaussian line source. The problem of infinite temperature at the beam impingement point in this model was solved in the SAE model by introducing an arbitrary plane above the actual plane. This means that a beam impinges on a plane at a distance $z_0$ above the plane, as shown in Fig. 1. This distance is determined so that heat diffusion from the arbitrary plane during injection time raises the actual surface temperature to a value which is equated to a known value as determined by the Bass equations [7]. Thus the surface temperature is limited to a finite value due to introduction of this arbitrary plane.

**Fig. 1**. Surface melting by a moving laser beam on an arbitrary plane at a distance $z_0$ above the actual plane

The temperature field equation for a Gaussian line source as given by the SAE model is as follows:

$$T - T_0 = \frac{Aq}{2\pi k v \sqrt{t(t+t_0)}} \exp\left[-\frac{1}{4\alpha}\left\{\frac{(z+z_0)^2}{t} + \frac{y^2}{(t+t_0)}\right\}\right] \qquad (1)$$

The symbols used in this work are given in Table 1, while the thermophysical data of Inconel 625 is detailed in Table 2.

Table 1 Symbols used

Table 2 Values and properties used for Inconel 625

## 4. Modelling different beam geometries

Shercliff et al. [5] have demonstrated how to use the SAE model for non-Gaussian as well as Gaussian sources. Any required beam profile can be simulated by superposition of Gaussian sources, as the differential heat flow equations are linear.

Fig. 2 shows the three different arrangements of sources used for the modelling work. The dimensions of the modelled beams were chosen so that each beam area was equivalent to that of the experimental beam. The modelled beams consist of: (1) a single circular source with r=2.4 mm, (2) three superimposed circular sources in a single row with r=1.5 mm and a power share of 40-20-40 percent, and (3) ten superimposed circular sources in a two-dimensional array with r=1 mm and a power share of 10 percent each. The single source (circular), 3-source (rectangular), and 10-source (rectangular) arrays will be referred to as 1C, 3R and 10R respectively.

**Fig. 2**. Arrangement of sources in the modelling work; (a) single circular source 1C, (b) 3-source rectangular beam 3R, (c) 10-source rectangular beam 10R

Fig. 3 shows the power density distribution for 1C, 3R and 10R beam profiles. In the present case, both rectangular beams present a top-hat profile in y-z plane and a Gaussian profile in x-z plane similar to the experimental beam. The 10R beam is more uniform in comparison with other beams due to the 2-D spatial arrangement of sources. It should be noted that a different set of spatial locations and/or power-share of individual Gaussian sources would produce a different profile, and these can be adjusted to match any desired beam profile.

**Fig. 3**. Power density distribution for Gaussian and non-Gaussian rectangular beams; 3-D and plan views; the numbers in plan views represent the percentage of power of each source; (a) 1C, (b) 3R, (c) 10R

The temperature field solution from the SAE model, Eq. (1), can be modified to the following expression for 3-sources beam. The terms are added due to the linearity of the model [5].

$$T - T_0 = \frac{A\exp[-\frac{(z+z_0)^2}{4\alpha t}]}{2\pi k v\sqrt{t(t+t_0)}}[\frac{q_1}{\exp[y_1^2/4\alpha(t+t_0)]} + \frac{q_2}{\exp[y_2^2/4\alpha(t+t_0)]} + \frac{q_3}{\exp[y_3^2/4\alpha(t+t_0)]}] \quad (2)$$

For the 2-dimensional array of the 10R beam, the contribution of individual sources offset by $\delta x$ in the beam travel direction is accounted for by a time shift $\delta t$, i.e. $t = t + \delta t$; where $\delta t = \frac{\delta x}{v}$. An offset of 1mm was used for the 10R beam. The temperature field equation then can be modified into the following expression where the sources $q_1$ to $q_5$ are not offset, while sources $q_6$ to $q_{10}$ include an offset due to their spatial location.

$$T - T_0 = \frac{A\exp[-\frac{(z+z_0)^2}{4\alpha t}]}{2\pi k v\sqrt{t(t+t_0)}}[\frac{q_1}{\exp[y_1^2/4\alpha(t+t_0)]} + \frac{q_2}{\exp[y_2^2/4\alpha(t+t_0)]} + .....\frac{q_5}{\exp[y_5^2/4\alpha(t+t_0)]}] +$$

$$\frac{A\exp[-\frac{(z+z_0)^2}{4\alpha(t+\delta t)}]}{2\pi k v\sqrt{(t+\delta t)[(t+\delta t)+t_0]}}[\frac{q_6}{\exp[y_6^2/4\alpha(t+\delta t+t_0)]} + \frac{q_7}{\exp[y_7^2/4\alpha(t+\delta t+t_0)]} + ....\frac{q_{10}}{\exp[y_{10}^2/4\alpha(t+\delta t+t_0)]}] \quad (3)$$

The SAE model was written in MatLab code and run for each of the three beam profiles.

## 5. Results

### *5.1 Validation of code*

It was important to validate the MatLab version of the model. This was done by reproducing one of the original 'master plots' presented by Shercliff et al. [5, 11]. Fig. 4 has been plotted using the 1C modelled beam and is an exact replica of Fig. 7 in reference [5], thus validating the MatLab model. This figure shows relationship of variables $z_c$* (dimensionless case depth) and v* (dimensionless speed) with contours of constant q* (dimensionless power) for laser hardening of medium carbon steel with a single Gaussian source.

**Fig. 4**. Replication of plot from [5] to validate the model

*5.2 Melt depth and melt pool profile*

The expressions used to calculate melt pool depth and profile are presented in the appendix. The latent heat correction was applied as suggested by Ashby et al [4], in which a fraction of energy (absorbed during melting) was subtracted from incident energy. The melt depth was calculated using Eqs. (A.1-A.3). Fig. 5 shows a comparison between experimental and predicted melt depths for different modelled beams for a given power setting. It also shows the effect of the chosen value of absorptivity for different scan speeds.

**Fig. 5**. Comparison of maximum melt depth between experimental data and model predictions showing effect of beam scan speed and absorptivity value; q=1500 W (a) A=0.5, (b) A=0.35

However, it is the melt pool shape that would determine the degree of overlap in multi scan applications. Fig. 6 shows the predicted melt pool boundary in the transverse cross section (y-z, plane perpendicular to the beam travel direction) for the different modelled beams. Every point on the curves corresponds to the melting temperature, i.e. 1623 K. The Gaussian (1C) and rectangular (3R and 10R) beams produced different melt shapes due to the selection of beam geometries which was based on equalisation of beam area. It also demonstrates the effect of beam scan speed on the shape of melt track; the rectangular beams produced a wider, top-hat shaped profile at higher scan speed, while the track produced by Gaussian beam remained unchanged at all speeds.

**Fig. 6**. Predicted melt pool track for different beams; A=0.5, q=1500 W, (a) v=1000 mm $min^{-1}$, (b) v=2000 mm $min^{-1}$

Fig. 7 shows a comparison of the experimentally obtained and modelled melt pools for different scan speeds. The experimental work showed that the melt pool was crescent-shaped for low speeds; and became more uniform (i.e. top-hat) for higher scan speeds. The modelled results for the rectangular beams successfully predicted this trend.

**Fig. 7**. Comparison of experimental and modelled melt pool profiles.

## 6. Discussion

Fig 5 shows that all three modelled beams successfully predict the experimentally observed trend of decreasing melt depth with increasing beam traverse speed. It can also be seen how the match between modelled and experimental melt depth results can be optimised by adjusting the value of absorptivity. An absorptivity of 0.35, i.e. 35%, was found to be appropriate for the Inconel 625 material used in the present work. This is a reasonable value for a nickel based alloy irradiated with a 940nm wavelength laser beam [12].

Fig. 7 showed that the predicted melt pool pattern produced by the rectangular beams had more resemblance with the experimental work than the circular beam, i.e. the model successfully predicts the effect of beam profile on melt pool shape. The melting temperature isotherms for 1C beam remained crescent-shaped at all speeds. The rectangular beams produced a top-hat shape at higher speeds and a crescent shape at slow speed, as was seen experimentally.

Information regarding the development of the melt pool can be obtained by considering the progression of predicted melt fronts along width and depth as function of time (at a specific scan speed) as shown in Fig. 8 and Fig. 9. The melt fronts are represented in terms of melting temperature contours, i.e. they are the locus of points at which $T=T_m$ at different positions for the stated time values. In these figures, the melt pool depth and width both increase initially as time increases (indicated by solid lines). The width reaches a maximum value at some time during progression (indicated by solid bold line). After this stage, pool depth increases while the width starts to decrease with time (indicated by dotted lines). This profile continues until the maximum melt depth is achieved (indicated by dotted bold line). The melt pool boundary then starts to shrink in both width and depth until the temperature falls below the melting point. Thus, the resultant melt pool boundary is the combined effect of these fronts at different time values.

**Fig. 8**. Predicted melt pool progression for 1C beam at low (1000 mm $min^{-1}$) and high scan speeds (2000 mm $min^{-1}$); A=0.5, q=1500 W; all contour points represent melting point

It can be seen that the 1C beam produced crescent-shape profiles at all speeds, as if the heat flow was always in two dimensions, i.e. y-direction and z-direction. However, the melt fronts advanced differently in 3R beam (Fig. 9). At high speed, the 3R beam melt fronts were approximately top hat shaped as would be in case of 1-dimensional heat conduction. At low speed, they initially started with a top hat shape which continued until the maximum melt width was reached. The second part of progression indicates that slow speed allowed enough time for heat to diffuse in 2-dimensions, thus changing the shape of the contour. As a result, a crescent-shape melt pool was obtained for the 3R beam at slow speed.

**Fig. 9**. Predicted melt pool progression for 3R beam at low (1000 mm $min^{-1}$) and high (2000 mm min-$^{1}$) scan speeds; A=0.5, q=1500 W; all contour points represent the melting point

Surface treatment operations such as transformation hardening and surface melting require large area processing, thus requiring several scans of laser beam. An overlap between the scans is required for uniformity of the treated region. The knowledge of relationship between beam geometry, process parameters and resultant melt pool can be utilised to optimise the overlap ratio in the experimental work, as indicated in Fig. 10. A smaller degree of overlap will lead to more efficient processing. It is clear from the above results that a rectangular beam is preferred over a circular beam in order to produce a more uniform surface treatment with minimal overlapping required. The model presented in this work can be usefully employed when determining the overlap required in various surface treatment processes.

**Fig. 10**. Overlap ratio for multi-pass operations; (a) non-uniform (Gaussian) beam requiring several passes, (b) uniform beam (rectangular) requiring few passes

The SAE model is based on heat transfer by conduction only; and completely ignores any effects caused by fluid flow and convection. Marangoni convection can significantly change the heat transfer behaviour in the melt pool and therefore change its shape [13]. Safdar et al.[14] compared the melt depths obtained from heat transfer and fluid flow models; and found that melt pool depth predicted by the heat transfer model alone was over estimated by several times. However, the melt pool

profile became flatter, i.e. similar to the experimental profile upon inclusion of fluid flow in the model. The diminishing difference in melt depth between experimental and modelling work with increased scanning speed seen in our results can again be attributed to the relationship of Marangoni convection and scanning speed. The strength of Marangoni forces depends on the temperature gradient within the melt pool which is controlled by heat input to the material. Higher beam scanning speeds result in lower heat input per unit length. This leads to lower temperature gradients and reduced Marangoni forces. The better match between experimental and modelled results at higher scanning speeds is therefore attributed to the reduced effect of Marangoni forces under these conditions.

In common with the original SAE model [4, 5], this work has not taken into account any temperature dependence of the thermal diffusivity, and has used room temperature values. In reality, thermal diffusivity is temperature dependent. The behaviour before melting is material dependent, however an increase with increasing temperature is typical for the Ni based superalloy, Inconel 625, considered in this work [12]. On melting there is a general decrease in thermal diffusivity due to the loss of the lattice phonon contribution to thermal conductivity. Such a decrease in thermal diffusivity would make the heat flow become more 1D. This would change the melt pool shape so that it becomes more uniform and flat bottomed, producing a better match between modelled and experimental results (Fig. 7). Therefore, this model could be improved by inclusion of this temperature dependency directly or, more simply, via an appropriately averaged value.

## 7. Conclusions

Superposition of Gaussian sources in the SAE model can replicate non-Gaussian beam geometries.

The model produced successfully predicts the trends of decreasing melt depth and the change in shape of melt pool with increasing laser beam traverse speed.

The value of absorptivity used in the model can be used as a fitting parameter to optimise agreement between modelled and experimental results. The model can then be used to predict the dimensions of the melt pool, and is thus a useful tool for determining overlap required in laser surface treatment processes.

An absorptivity value of 0.35 (35%) is suitable for Inconel 625 irradiated with a 940nm wavelength laser beam.

The model is most successful in conditions where Marangoni effects are minimal, i.e. where there is no melting or where the melt pool has a top hat shape, such as is obtained when the laser traverse speed is high.

It should be noted that though the model is applied to laser surface melting in this work, it would also be a useful tool for other laser surface applications such as laser transformation hardening.

**Appendix**

*Single source:*

$$z_m = \sqrt{-4\alpha t(\ln[\frac{2\pi kv\sqrt{t(t+t_0)}(T_m - T_0)}{Aq}] + \frac{y^2}{4\alpha(t+t_0)})} - z_0 \qquad \text{(A.1)}$$

*Three sources in 1-D array*:

$$z_m = \sqrt{-4\alpha t(\ln[\frac{2\pi kv\sqrt{t(t+t_0)}(T_m - T_0)}{A[\frac{q_1}{\exp[y_1^2/4\alpha(t+t_0)]} + \frac{q_2}{\exp[y_2^2/4\alpha(t+t_0)]} + \frac{q_3}{\exp[y_3^2/4\alpha(t+t_0)]}]}])} - z_0 \qquad \text{(A.2)}$$

*Ten sources in 2-D array*:

$$z_m = \sqrt{-4\alpha[roots\,of\ f(X_3)]} - z_0 \qquad \text{(A.3)}$$

where $f(X_3) = \frac{X_1 \exp[\frac{X_3}{t}]}{\sqrt{t(t+t_0)}} + \frac{X_2 \exp[\frac{X_3}{t+\delta t}]}{\sqrt{(t+\delta t)[(t+\delta t)+t_0]}} - \frac{2\pi kv(T_m - T_0)}{A}$

The values of $X_1$ and $X_2$ correspond to sources without and with x-offset respectively; and are given by the following expressions:

$$X_1 = [\frac{q_1}{\exp[y_1^2/4a(t+t_0)]} + \frac{q_2}{\exp[y_2^2/4a(t+t_0)]} + .....\frac{q_5}{\exp[y_5^2/4a(t+t_0)]}]$$

$$X_2 = [\frac{q_6}{\exp[y_6^2/4a(t+\delta t+t_0)]} + \frac{q_7}{\exp[y_7^2/4a(t+\delta t+t_0)]} + .....\frac{q_{10}}{\exp[y_{10}^2/4a(t+\delta t+t_0)]}]$$

$$X_3 = \frac{-(z+z_0)^2}{4\alpha}$$

## References

[1] Z. Liu, P. H. Chong, P. Skeldon, P. A. Hilton, J. T. Spencer and B. Quayle, Surface and Coatings Technology 200 (2006) 5514.
[2] K. G. Watkins, Z. Liu, M. McMahon, R. Vilar and M. G. S. Ferreira, Materials Science and Engineering A A252 (1998) 292.
[3] P. H. Chong, Z. Liu, X. Y. Wang and P. Skeldon, Thin Solid Films 453-454 (2004) 388.
[4] M. F. Ashby and K. E. Easterling, Acta Metallurgica 32 (1984) 1935.
[5] H. R. Shercliff and M. F. Ashby, Metallurgical Transactions A (Physical Metallurgy and Materials Science) 22A (1991) 2459.
[6] N. Rykalin, A. Uglov and A. Kokora, Laser Machining and Welding (Pergamon Press, 1978).
[7] M. Bass, in "Physical Processes in Laser-Materials Interactions", edited by M. Bertolotti (Plenum Press, 1983) p. 77.
[8] C. Hu and T. N. Baker, Acta Metallurgica et Materialia 43 (1995) 3563.
[9] R. C. Reed, Z. Shen, J. M. Robinson and T. Akbay, Materials Science and Technology 15 (1999) 109.
[10] J. C. Ion, H. R. Shercliff and M. F. Ashby, Acta Metallurgica et Materialia 40 (1992) 1539.
[11] H. R. Shercliff and M. F. Ashby, The prediction of case depth in laser transformation hardening, (Cambridge University Engineering Department; Report number CUED/C-Mat./TR169 1989).
[12] A. Hazotte, B. Perrot and P. Archambault, Journal de Physique IV 3 (1993) 351.

**Vitae**

Dr Nauman Ahmed works in the general area of coatings and corrosion. He obtained his PhD “Characterisation of Different Forms of Inconel 625 for Determining the Effects of Microstructural Modifications on Electrochemical Behaviour” in 2008 at the University of Nottingham.

Dr Katy Voisey is a lecturer at the University of Nottingham. Her research interests are based on the three main areas of laser material processing, coatings and corrosion. Current projects include fibre laser cutting and the use of electrochemical methods to study corrosion of thermally sprayed coatings.

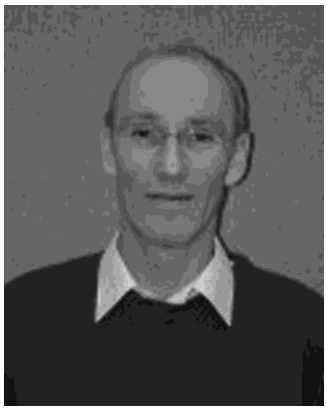

Prof D.G. McCartney undertakes both fundamental and applied research in the field of processing of engineering materials. He has a number of research projects concerned with the development of new and improved coatings to protect engineering coatings against aggressive wear, corrosion or high temperature oxidation and to provide novel properties. Prof McCartney is also interested in the use of intense power sources such as lasers or electric arcs for joining of advanced alloys and direct metal deposition (additive manufacture) to produce high performance components for a range of engineering applications.

## Figures

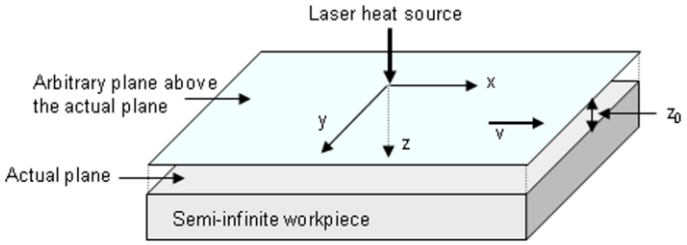
Laser heat source
Arbitrary plane above
the actual plane
Actual plane
Semi-infinite workpiece
x
y
z
v
$z_0$

1

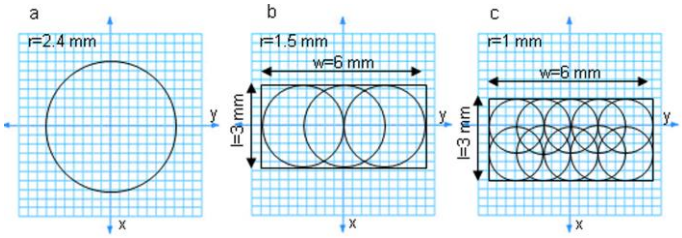
a
r=2.4 mm
b
r=1.5 mm
w=6 mm
l=3 mm
c
r=1 mm
w=6 mm
l=3 mm
x
y

2

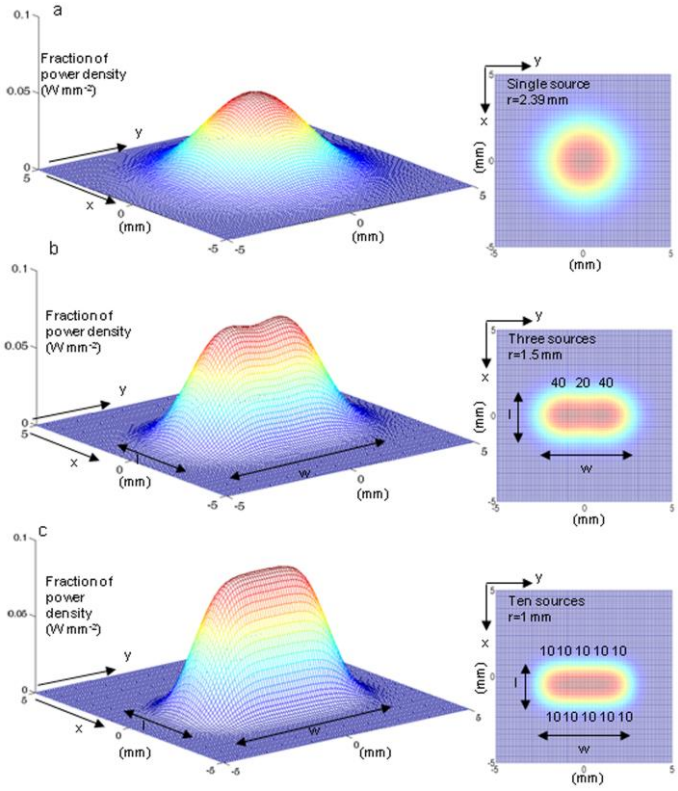
a
Fraction of
power density
(W mm⁻²)
Single source
r=2.39 mm
b
Three sources
r=1.5 mm
40 20 40
c
Ten sources
r=1 mm
10 10 10 10 10
10 10 10 10 10
x
y
l
w
(mm)

3

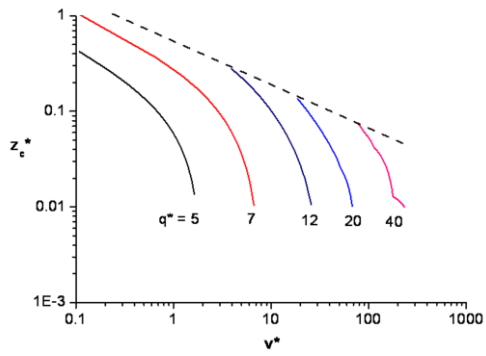
1
0.1
0.01
1E-3
$z_c^*$
q* = 5
7
12
20
40
0.1
1
10
100
1000
v*

4

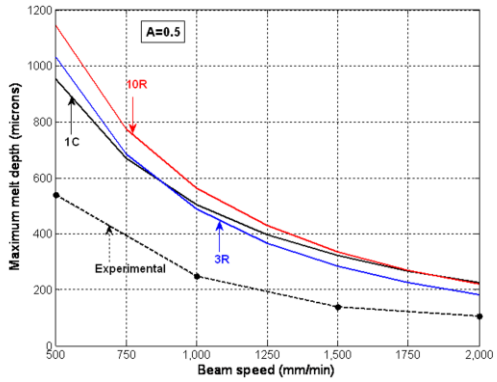
A=0.5
10R
1C
3R
Experimental
Maximum melt depth (microns)
Beam speed (mm/min)
1200
1000
800
600
400
200
0
500
750
1,000
1250
1,500
1750
2,000

5a

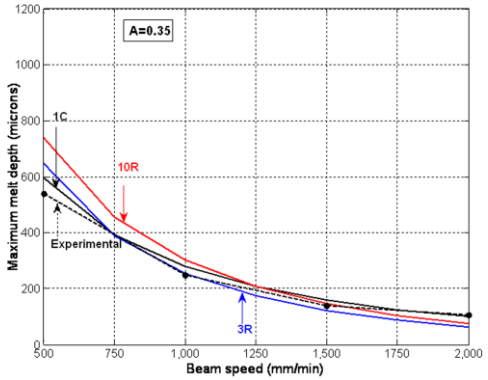
A=0.35
1C
10R
Experimental
3R
Maximum melt depth (microns)
Beam speed (mm/min)
1200
1000
800
600
400
200
0
500
750
1,000
1250
1,500
1750
2,000

5b

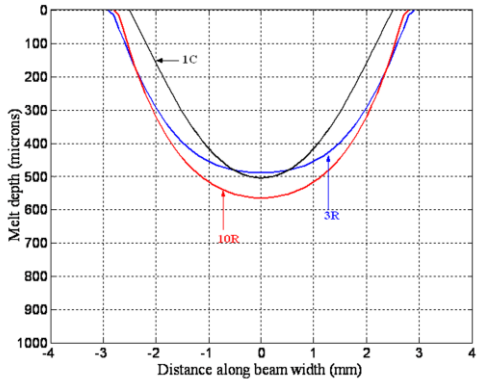
1C
3R
10R
Melt depth (microns)
Distance along beam width (mm)

6a

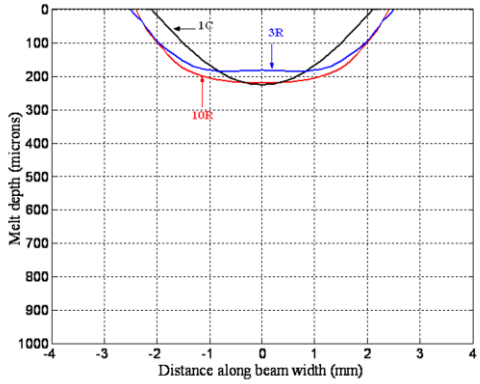
1C
3R
10R
Melt depth (microns)
Distance along beam width (mm)

6b

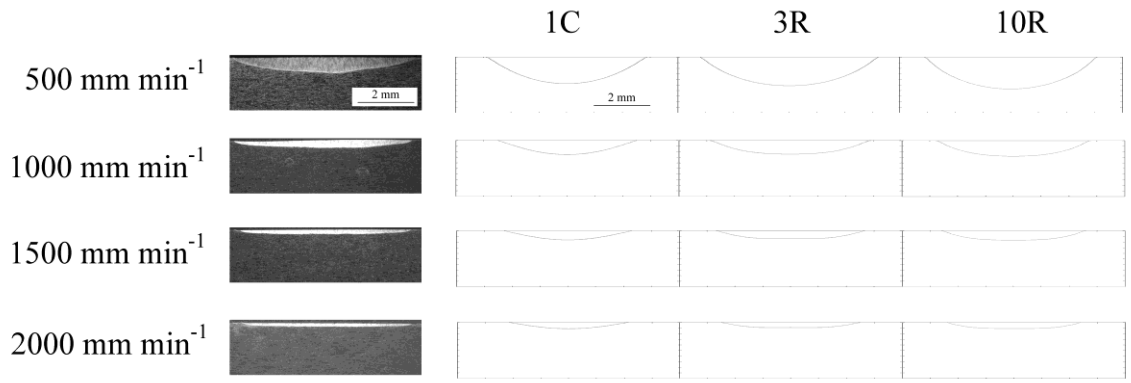
1C
3R
10R
500 mm min-1
1000 mm min-1
1500 mm min-1
2000 mm min-1
2 mm
2 mm

7

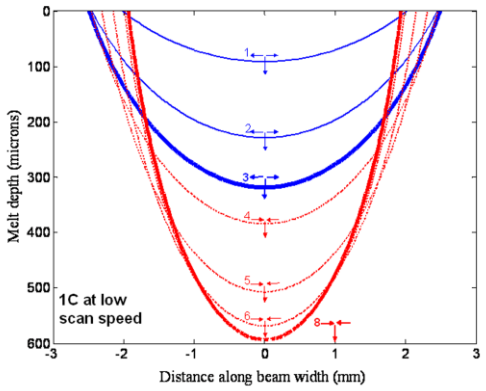
Melt depth (microns)
Distance along beam width (mm)
1C at low
scan speed
1
2
3
4
5
6
8

8a

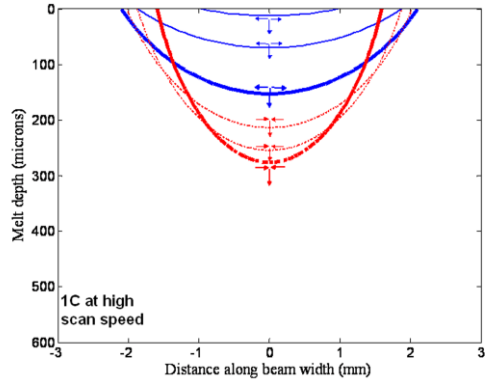
Melt depth (microns)
Distance along beam width (mm)
1C at high
scan speed

8b

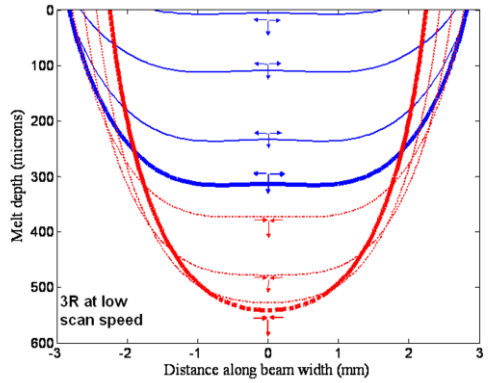
Melt depth (microns)
Distance along beam width (mm)
3R at low
scan speed

9a

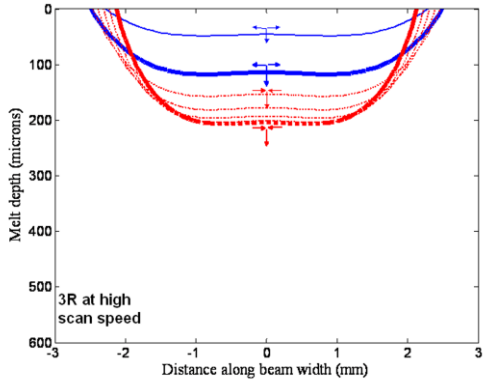
Melt depth (microns)
Distance along beam width (mm)
3R at high
scan speed

9b

10a

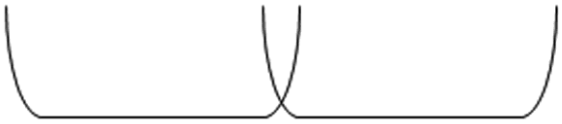

10b

**Legends**

**Fig. 1** Surface melting by a moving laser beam on an arbitrary plane at a distance $z_0$ above the actual plane

**Fig. 2** Arrangement of sources in the modelling work; (a) single circular source 1C, (b) 3-source rectangular beam 3R, (c) 10-source rectangular beam 10R

**Fig. 3** Power density distribution for Gaussian and non-Gaussian rectangular beams; 3-D and plan views; the numbers in plan views represent the percentage of power of each source; (a) 1C, (b) 3R, (c) 10R

**Fig. 4** Replication of plot from [5] to validate the model

**Fig. 5** Comparison of maximum melt depth between experimental data and model predictions showing effect of beam scan speed and absorptivity value; q=1500 W (a) A=0.5, (b) A=0.35

**Fig. 6** Predicted melt pool track for different beams; A=0.5, q=1500 W, (a) v=1000 mm $min^{-1}$, (b) v=2000 mm $min^{-1}$

**Fig. 7** Comparison of experimental and modelled melt pool profiles.

**Fig. 8** Predicted melt pool progression for 1C beam at low (1000 mm $min^{-1}$) and high scan speeds (2000 mm $min^{-1}$); A=0.5, q=1500 W; all contour points represent melting point

**Fig. 9** Predicted melt pool progression for 3R beam at low (1000 mm $min^{-1}$) and high (2000 mm $min^{-1}$) scan speeds; A=0.5, q=1500 W; all contour points represent the melting point

**Fig. 10** Overlap ratio for multi-pass operations; (a) non-uniform (Gaussian) beam requiring several passes, (b) uniform beam (rectangular) requiring few passes

## Tables

Table 1 Symbols used

| | | |
|---|---|---|
| A | Surface absorptivity | |
| $I_0$ | Laser beam intensity | $Wm^{-2}$ |
| k | Thermal conductivity | $Js^{-1}m^{-1}K^{-1}$ |
| L | Latent heat of fusion per unit volume | $Jm^{-3}$ |
| l | Beam length | m |
| q | Laser power | W |
| r | Laser beam radius | m |
| T | Temperature | K |
| $T_0$ | Initial temperature | K |
| $T_m$ | Melting temperature | K |
| t | Time | s |
| v | Beam scan speed | $ms^{-1}$ |
| w | Beam width | m |
| x, y, z | Cartesian co-ordinates | m |
| $z_0$ | Calibration distance over which heat diffuses during interaction time | m |
| $z_m$ | Maximum melt depth | m |
| α | Thermal diffusivity | $m^2s^{-1}$ |
| $t_0$ | Time taken for heat to diffuse over a distance equal to the beam radius | s |

Table 2 Values and properties used for Inconel 625

| | |
|---|---|
| Absorptivity[1] | A= 0.5 |
| Specific heat | $C_p$=410 $Jkg^{-1}K^{-1}$ |
| Thermal conductivity | k=9.8 $Wm^{-1}K^{-1}$ |
| Latent heat of fusion per unit volume[2] | L=1.726 x $10^9$ |
| Initial temperature | $T_0$=300 K |
| Melting temperature | $T_m$=1623 K |
| Density | ρ=8440 $kgm^{-3}$ |

[1] *Approximate value chosen based on different values used in the literature*

[2] *Determined experimentally by Differential Scanning Calorimetry (SDC) method*